

# Analysis of Streamer Propagation for Electric Breakdown in Liquid/Bioliquid

Yong Yang, Andrey Starikovskiy, Alexander Fridman, & Young I. Cho\*

Department of Mechanical Engineering and Mechanics, Drexel University, Philadelphia, PA

\*Address all correspondence to: Young I. Cho, Department of Mechanical Engineering and Mechanics, Drexel University, Philadelphia, PA 19104; Tel.: +1-215-895-2425; Fax: +1-215-895-1478; choyi@drexel.edu

**ABSTRACT:** There is an increasing interest in the study of direct plasma generated in liquid/bioliquid as it finds more applications in both industry and academic research. For all the applications, it is important to get a better understanding of the key physical mechanisms of the breakdown process. In the present paper, streamer propagation during an electric breakdown process of dielectric liquid was analyzed quantitatively using two different mechanisms based on electrostatic expansion and local heating. It was proposed that at the early stage of the streamer propagation, the electrostatic force due to the charging of a liquid-gas interface under a high electric field might be the major driving force for filament growth. Over a submicro-second time scale, the local heating might dominate the streamer propagation process, and the growth of the filament could be caused by the continuous evaporation of liquid at the tip of the streamer. Analysis of linear instabilities that lead to the bushlike growth of the streamers was carried out. Both classic Rayleigh-Taylor instability and electric field-induced instability were identified. It was shown that with an increasing applied voltage, the electrostatic instability was enhanced, whereas the Rayleigh instability was suppressed.

**KEY WORDS:** electric breakdown, plasma, streamer propagation, stability analysis, Rayleigh instability

## NOMENCLATURE

$c_p$  specific heat,  $C$  speed of sound,  $e$  electron charge,  $E$  electric field,  $h$  peak-to-peak amplitude,  $H$  depth of wave influence,  $k$  wave number,  $k_i$  ionization rate coefficient,  $L$  length,  $m$  mass,  $M$  Mach number,  $n$  number density,  $P$  pressure,  $R$  interelectrode distance,  $r$  radius,  $u$  velocity,  $V$  volume,  $t$  time,  $T$  temperature,  $Z$  internal energy, **Greek Symbols:**  $\alpha$  specific heat ratio,  $\gamma$  surface tension,  $\Delta_v H$  evaporation heat of water,  $\epsilon$  permittivity,  $\kappa$  electric conductivity,  $\lambda$  thermal conductivity,  $\rho$  density,  $\sigma$  surface charge density,  $\tau$  time,  $\nu$  collision frequency,  $\tau$  time constant,  $\Phi$  voltage,  $\omega$  oscillation frequency,  $\chi$  curvature, **Subscripts:** b breakdown, c crest, e electron, E electrostatic, I ionization, HD hydrodynamic, n neutral, t trough, T tension.

## I. INTRODUCTION

There is an increasing interest in the study of electric breakdown in water and other liquids as it finds more applications in both industry and academic research, ranging from dielectric insulation to water sterilization, organic contaminants destruction, and material synthesis.<sup>1–6</sup> For all the applications, it is important to get a better understanding of the key physical mechanisms of the breakdown process. In most cases, the electric

breakdown of liquids is initiated by the application of a high electric field on the electrode, followed by rapid propagation and branching of streamers. The overall mechanism is complex since it involves different physical processes including field emission, bubble formation, ionization, heating, vaporization, etc. Thus, it is difficult to include all the effects in a single analytical model. A number of proposed theories for the initiation of the breakdown of dielectric liquids are available in the literature.<sup>7–12</sup> The initial bubble formation could be attributed to pre-existing cavities in water, direct ionization, field-assisted emission, or joule heating induced by local field emission. However, the exact mechanism is still unclear.

Despite different mechanisms proposed, all the initiation theories lead to the formation of a low-density region so that self-sustained electron avalanche could be possible. Thus, the next question is what the driving force is to sustain and expand the cavity to form complex geometrical structures. Similar to the initiation process, the propagation is complicated because it involves interactions between plasma, gas, and liquid phases of the media. Recent experiments demonstrated the existence of different modes of propagation where both a primary streamer mode with a slow velocity and a secondary streamer mode with a high velocity were observed.<sup>13</sup> Several models have been proposed to correlate the electric field to streamer velocity.<sup>14–16</sup> Different effects, including liquid viscosity, trapping of positive and negative carriers in the conducting channel, and local electric charge at the streamer head, were taken into account. But again, there is not yet a commonly accepted model.

The objective of the present study was to develop a theoretical framework for understanding the propagation of streamers of electric discharge in water subjected to high voltage. The breakdown process is usually characterized by two typical features of breakdown, namely, the rapid propagation of discharge streamers and high tendency of branching and formation of random dendritic structures. Therefore, the present study consists of two components, i.e., a quantitative model for possible mechanisms to produce the driving force needed to sustain and promote the propagation, and a stability analysis of a single cylindrical filament with surface charges in an external electric field.

## II. MODELS

Despite the fact that the mechanism is not fully understood, the propagation of streamers during electric breakdown of water clearly involves the displacement of adjacent liquid along their paths. The process requires a driving force, which is to be discussed in this section. Two quantitative models have been developed. One is based on the electrostatic effect on the streamer-water interface, and the other a more traditional local heating effect. Comparison was made to examine the validities of the two models.

### A. Electrostatic Model

A schematic diagram of the present electrostatic model is shown in Figure 1A. A thin needle electrode with a rounded tip was aligned perpendicular to a ground plate elec-

trode. High voltage  $\Phi_0$  was applied to the needle electrode. According to Kupershtokh et al., liquids could become phase unstable under a high electric field so that gas channels could form along electric field lines.<sup>17</sup> The time required for breakdown ignition in the channels can be estimated as  $\tau_b = (k_i n_0)^{-1}$ , where  $k_i$  is the direct ionization rate coefficient, and  $n_0$  is the molecule density.<sup>18</sup> Under atmospheric pressure,  $n_0$  is on the order of  $10^{19} \text{ cm}^{-3}$ , while  $k_i$  is on the order of  $10^{-10}$  to  $10^{-9} \text{ cm}^3/\text{s}$  in the reduced electric field  $E/n_0$  of  $10^3 \text{ V}\cdot\text{cm}^2$ .<sup>18</sup> Hence,  $\tau_b$  is on the order of 0.1 to 1 ns. For negative discharges, due to the higher momentum transfer collision frequency and thus a low mobility in the liquid phase, electrons tend to deposit on the gas-liquid interface and charge it negatively. For positive discharges, the high mobility of electrons would leave the interface charged positively. Under both circumstances, it is possible that the charged interface would be pushed to displace the liquid under an external electric field by electrostatic force. A simplified calculation can be made to examine whether or not the electrostatic force would be sufficient to overcome the resistance of water at the interface. The pressure due to the surface tension  $\gamma$  on a water interface of a spherical bubble with a radius of curvature  $r$  can be approximated by the Young-Laplace equation  $p = 2\gamma/r$ . With  $r \sim 1 \text{ }\mu\text{m}$ , and  $\gamma = 72.8 \times 10^{-4} \text{ N/m}$ , the surface tension pressure is  $\sim 15 \text{ kPa}$ . The ultimate strength of water of approximately 30 MPa must be exceeded for rupturing the liquid.<sup>19</sup> Considering forces due to charged particles only, and ignoring those due to field gradients and material property gradients, the electric force at the interface becomes simply the electrostatic force  $L$ , which is the product of charge density per unit area  $\sigma$  and the electric field  $E$ , i. e.,  $L = e\sigma E$ , where  $e$  is the charge per electron. For  $E = 10^8 \text{ V/cm}$ ,  $\sigma$  should have a value of  $10^{12} \text{ charges/cm}^2$ . For electrons with an average energy of 1 eV, the electron thermal velocity can be estimated as  $6 \times 10^7 \text{ cm/s}$ . So a modest electron density of  $10^{13} \text{ cm}^{-3}$  will provide the flux necessary to charge the surface to the breaking point within 1 ns. Although these estimations for water rupturing also neglect both loss mechanisms and the energy requirements to overcome the hydrodynamic resistance, the electrostatic mechanism still seems a likely candidate for streamer propagation, and such forces may dominate at a nanosecond time scale.

The growth of a plasma filament is determined by conservation equations of mass, momentum, and energy. To quantify the breakdown process described above, the equations for the formation and propagation of the plasma-filled filaments are defined as<sup>20</sup>

$$\frac{\partial \rho}{\partial t} + \nabla \cdot (\rho u) = \frac{2\lambda(T)T}{\Delta_\nu H r_0^2} \quad (1)$$

$$\frac{\partial u}{\partial t} + u \cdot \nabla u + \frac{1}{\rho} \nabla P = 0 \quad (2)$$

$$\frac{\partial}{\partial t} [\rho(Z + u^2)] + \nabla \cdot \left[ \rho u \left( \frac{P}{\rho} + \frac{u^2}{2} \right) \right] = \kappa(T) E^2 \quad (3)$$

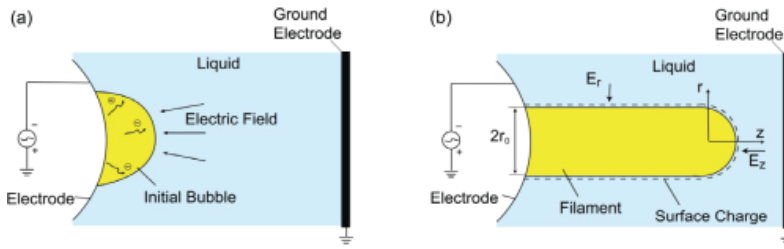


**FIGURE 1.** (A) Initiation of bubble formation; (B) schematic diagram of a cylindrical filament in water.

where  $t$  is time,  $\rho$  and  $P$  are the radial density and pressure inside streamer, respectively,  $u$  is the velocity of streamer,  $T$  is the temperature,  $\lambda$  is the thermal conductivity,  $\Delta_v H$  is the evaporation heat of water,  $r_0$  is the radius of streamer,  $Z$  is the internal energy of ionized gas,  $E$  is the electric field strength, and  $\kappa$  is the electric conductivity. It is usually difficult to directly solve Eqs. (1)–(3) because of the high nonlinearity of the equations.

For simplification, the streamer was assumed to be a cylinder with a hemispherical tip as shown in Figure 1B. The reference frame was fixed on the tip. The radius of the filament is  $r_0$ . Although it appears from photographic evidences that the filament is usually of a conical shape, the cylindrical approach is still a good approximation when the length of the filament is much greater than the radius. The electric conductivity  $\kappa$  inside the filament could be described as

$$\kappa = \frac{n_e e^2}{m v_{en}} \quad (4)$$

where  $m$  is the mass of electron, and  $v_{en}$  is the frequency of electron-neutral collisions. Note that  $v_{en}$  is proportional to the gas number density and the value of  $v_{en}/\rho$  is usually on the order of  $10^9 \text{ s}^{-1} \text{ Torr}^{-1}$ .<sup>18</sup> Sunka et al. measured the broadening of the  $H\alpha$  line profile, which is commonly used to characterize the density of plasma, reporting the electron density inside streamers during the initial phase of water breakdown to be on the order of  $10^{18} \text{ cm}^{-3}$ .<sup>21</sup> With the room temperature saturated water vapor pressure of 20 Torr, the electric conductivity inside the filament can be estimated to be on the order of  $10^7 \text{ S/m}$ , a value that is comparable to those for metals. Thus, the filament could be regarded as equipotential with the electrode, and thus could be treated as an extension of the electrode throughout the expansion. The external fluid provides drag force and constant external pressure for the development of the filament. Gravity is neglected here because the body force induced by gravity is much smaller than the electric forces.

The electric field outside a slender jet can be described as if it were due to an effective linear charge density (incorporating the effects of both free charge and polarization charge) of charge density  $\sigma$  on the surface. Since the charge density in liquid can be ignored compared to that on the filament surface, one can have the following equation for the space outside the filament by applying the Laplace equation in the radial direction:

$$\frac{1}{r} \frac{\partial}{\partial r} \left( r \frac{\partial \Phi}{\partial r} \right) = 0 \quad (5)$$

with boundary conditions  $\Phi|_{r=r_0} = \Phi_0$  and  $\Phi|_{r=R} = 0$ .  $R$  is the distance between the anode and cathode. Because the filament could be regarded as an extension of the electrode,  $R$  decreases as the streamer propagates through the gap.

Solving the above equation with an assumption of negative discharge, the radial electric field  $E_r$  and local surface charge density  $\sigma_r$  can be written as

$$E_r = \frac{\partial \Phi}{\partial r} = - \frac{\Phi_0}{r_0 \ln(R / r_0)} \quad (6)$$

$$\sigma_r = \varepsilon E_r = - \varepsilon_r \varepsilon_0 \frac{\Phi_0}{r_0 \ln(R / r_0)} \quad (7)$$

There is no analytical solution for the electric field at the hemispherical tip of the filament. A frequently used approximation is  $E_z \approx \Phi_0 / r_0$ . Here, the equation for the electric field at the tip of a needle in a needle-to-plane geometry developed by Lama and Gallo was used,<sup>22</sup>

$$E_z = - \frac{2\Phi_0}{r_0 \ln(4R / r_0)} \quad (8)$$

Similarly, the local charge density at the tip is:

$$\sigma_z = \varepsilon E_z = - \varepsilon_r \varepsilon_0 \frac{2\Phi_0}{r_0 \ln(4R / r_0)} \quad (9)$$

From Eqs. (6)–(9), one can conclude that the radial direction electrostatic pressure  $E\sigma$  exerted on the sidewall of the streamer was weaker than the axial direction electrostatic pressure on the tip. Note that both electrostatic pressures were roughly inversely proportional to  $r_0^2$ , meaning that at the initial stage of the filament growth when  $r_0$  is small, the electrostatic forces on both directions were strong and the filament would grow both axially and radially. A direct consequence of both the axial and radial expansions of the streamer channel is the launching of compression waves into adjacent liquids.<sup>13</sup> At some critical point, the electrostatic force would reach a balance with hydrodynamic resistance acting on the surface in the radial direction first, while the filament continued to grow in the axial direction.

Experimentally recorded propagation speeds of the filaments varied depending on the measurement techniques, ranging from a few kilometers to one hundred kilometers per second.<sup>13,23,24</sup> In spite of the discrepancy observed by different groups, the propagation was clearly in the supersonic regime, and the formation of shockwaves had to be taken into consideration (see Fig. 2). The drag force on the tip of the streamer, which is a stagnation point, equals to the force produced by the total hydrodynamic pressure,

$$P_{hd} = P_1 \left( \frac{2\alpha}{\alpha + 1} M_1^2 - \frac{\alpha - 1}{\alpha + 1} \right) + \frac{1}{2} \rho (CM_2)^2 \quad (10)$$

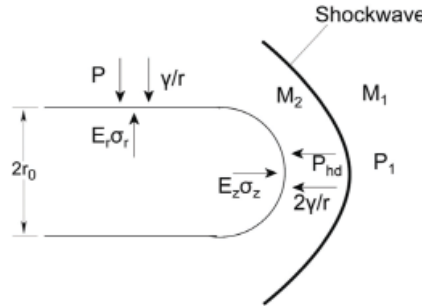


**FIGURE 2.** Force balance for the present electrostatic model.

where  $P_1$  is ambient pressure,  $P_1 \cdot \left( \frac{2\alpha}{\alpha+1} M_1^2 - \frac{\alpha-1}{\alpha+1} \right)$  is the pressure behind shock front,  $\alpha$  is the specific heat ratio of water,  $M_1$  is the Mach number of streamer,  $M_2$  is the Mach number after the shock front, and  $C$  is the speed of sound in liquid. The relationship between  $M_1$  and  $M_2$  can be written as<sup>25</sup>

$$M_2^2 = \frac{(\alpha-1)M_1^2 + 2}{2\alpha M_1^2 + 1 - \alpha} \quad (11)$$

Equating the hydrodynamic pressure to the sum of the electrostatic pressure and the pressure produced by surface tension at the tip can give the following equation for streamer propagation:

$$4\epsilon_r \epsilon_0 \frac{\Phi_0^2}{r_0^2 \ln^2(4R/r_0)} = P_1 \left( \frac{2\alpha}{\alpha+1} M_1^2 - \frac{\alpha-1}{\alpha+1} \right) + \frac{1}{2} \rho (CM_2)^2 + \frac{2\gamma}{r_0} \quad (12)$$

The balance between the electrostatic force and the force produced by the total hydrodynamic pressure in the radial direction can be given as

$$\epsilon_r \epsilon_0 \frac{\Phi_0^2}{r_0^2 \ln^2(R/r_0)} = P_1 + \frac{1}{2} \rho (CM_2)^2 + \frac{\gamma}{r_0} \quad (13)$$

Note that there are three unknowns,  $M_1$ ,  $M_2$ , and  $r_0$ , in the above equations. So it is possible to solve Eqs. (11)–(13) simultaneously when the applied voltage  $\Phi_0$  and the interelectrode distance  $R$  are specified.

To demonstrate the validity of the present model, the filament radius predicted by the model is shown in Figure 3. For a typical interelectrode distance of 1 cm, the filament radius increased from 3  $\mu\text{m}$  to 50  $\mu\text{m}$  as the applied voltage rose from 5 kV to 30 kV. The value was comparable to typical experimental values. For example, Baumung and Bluhm reported that the light emission from the discharge was restricted to a channel of 100  $\mu\text{m}$  diameter, indicating the interaction of charged particles in the region.<sup>13</sup>

Figure 4 shows the filament propagation speed as a function of  $\Phi_0$  and  $R$ . The calculated propagation speed from the present model was around 15 km/s, which was higher

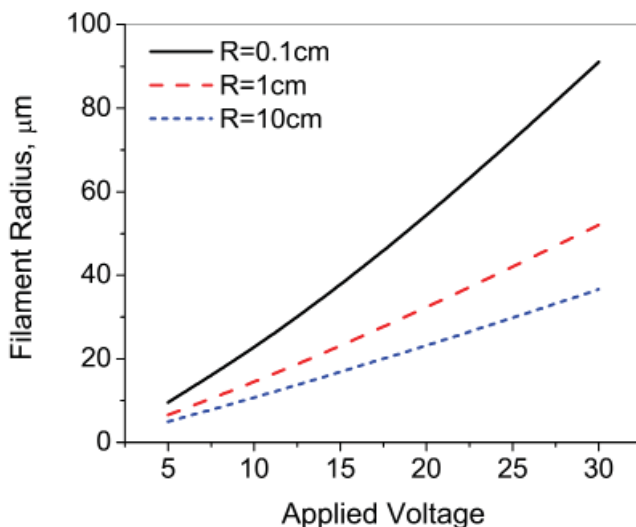


**FIGURE 3.** Variations of filament radius as a function of applied voltage and interelectrode distance.

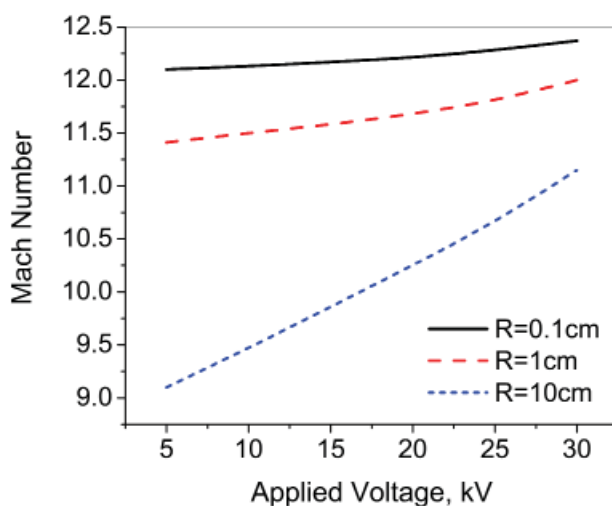


**FIGURE 4.** Variations of the Mach number of a streamer as a function of applied voltage and interelectrode distance.

than the primary streamer speed, but lower than the secondary streamer speed reported by Baumung and Bluhm.<sup>13</sup> The Mach number increased moderately with the applied voltage, a phenomenon that is understandable from the point of view of energy conservation. The streamer propagation velocity was relatively independent of the interelectrode distance. For an applied voltage of 30 kV, the Mach number increased from 11.2 to 12.3 when the interelectrode distance decreased from 10 cm to 0.1 cm. This is consistent



with the known property of negative streamers since the previous experiment showed that for a given voltage the propagation velocity was relatively constant as the streamer crossed the gap, and it increased as the streamer approached the plane electrode.<sup>14</sup> This phenomenon could be understood by Eq. (6), i.e., the interelectrode distance  $R$  was decreased with the propagation of the streamers; as a result, the electric field at the tip of the streamer was increased, leading to a higher propagation speed. However, the amount of the increase in the electric field would not be significant because of the natural logarithm in the equation.

## B. Thermal Mechanism

In the electrostatic model described above, it was assumed that the translational temperature inside the streamer was low, and the electrostatic force was the only driving force for the growth of the filament. The assumption was valid only at the initial stage of the filament development, since the temperature will keep rising as the molecules gain more energy through electron-neutral collisions. The heating time  $\tau$  is approximately  $\tau = \tau_{\text{en}} + \tau_{\text{vt}}$ , where  $\tau_{\text{en}}$  is the time for electron-neutral excitation, and  $\tau_{\text{vt}}$  is the time for vibrational-translational (v-t) relaxation. For electron-neutral excitation,  $\tau_{\text{en}} = 1/\nu_{\text{en}} = 1/(n_{\text{e}}k_{\text{en}})$ , where  $\nu_{\text{en}}$  is the electron-neutral nonelastic collision frequency,  $n_{\text{e}}$  is the electron density, and  $k_{\text{en}}$  is the rate constant for electron-neutral collisions;  $k_{\text{en}}$  can be expressed as  $k_{\text{en}} = \sigma_{\text{en}}\nu_{\text{te}}$ , where  $\sigma_{\text{en}}$  is the cross section for vibrational excitation of  $\text{H}_2\text{O}$  molecules by electron impact and  $\nu_{\text{te}}$  is the electron thermal velocity.

For electrons with an average energy of 1 eV, the cross section for vibrational excitation is about  $\sigma = 10^{-17} \text{ cm}^2$ .<sup>26</sup>  $k_{\text{en}}$  is thus about  $10^{-8} \text{ cm}^3/\text{s}$ , as is typical ( $\nu_{\text{te}} = 6 \times 10^7 \text{ cm/s}$ ). Spectroscopic measurements indicated that the stark broadening of the  $H\alpha$  line corresponded to an electron density of about  $10^{18} \text{ cm}^{-3}$  at a quasi-equilibrium state.<sup>21</sup> Thus, the typical electron-neutral excitation time can be estimated to be on the order of a few nanoseconds. For the v-t relaxation,  $\tau_{\text{vt}} = 1/(n_{\text{v}}k_{\text{vt}})$ , where  $n_{\text{v}}$  is the density of vibrational excited molecules, and  $k_{\text{vt}}$  is the v-t relaxation rate coefficient. For water molecules at room temperature,  $k_{\text{vt}}$  is about  $3 \times 10^{-12} \text{ cm}^3/\text{s}$ .<sup>18</sup> Assuming that  $n_{\text{v}}$  is on the same order with the electron density,  $\tau_{\text{vt}}$  could be estimated to be on the order of several hundred nanoseconds, suggesting that heating can take place inside the filaments under a submicrosecond time scale due to the energy transfer from the electrons to the translational energy of the water molecules; and furthermore, the propagation of the streamers could be caused by the continuous evaporation of water molecules at the tip. Here, the energy dissipation was not considered, and the actual heating time might be longer, but still the local heating mechanism under the submicrosecond time regime seems possible.

To quantify the process described above, it was assumed that a small cylindrical portion of water evaporated at the tip of the streamer during time  $\Delta t$  so that the length of the streamer grew from  $L$  to  $L + \delta L$ , as shown in Figure 5. The diameter of the evaporated water cylinder was assumed to be  $2r_{\text{e}}$ . There was no definitive value for pressure  $P_{\text{e}}$  inside the small vaporized portion given the extremely high temperature. However,  $P_{\text{e}}$  could be estimated to be on the order of 1000 atm because of the density difference





created by both surface tension and total environmental hydrodynamic pressure as given below,

$$P_0 = P_1 + \frac{1}{2} \rho (CM_2)^2 + \frac{\lambda}{r_0} \quad (19)$$

Another set of equations can be obtained through the consideration of energy conservation. The energy required to vaporize water was the electric energy provided by the power supply. If the entire filament was viewed as a capacitor with capacitance  $C$ , the required energy could be calculated as

$$E = \frac{C\Phi_0^2}{2} \quad (20)$$

The capacitance of the cylindrical filament is

$$C = 2\pi\epsilon\epsilon_0 L / \ln(R / r_0) \quad (21)$$

So the energy change required to extend the length by  $\delta L$  becomes

$$\delta E = \pi\epsilon\epsilon_0 \delta L \Phi_0^2 / \ln(R / r_0) \quad (22)$$

By equating  $\delta E$  to  $E_e$ , one has

$$r_e = \sqrt{\frac{\epsilon\epsilon_0 \Phi_0^2}{\rho(c_p \Delta T + \Delta H_{l-g}) \ln(R / r_0)}} \quad (23)$$

Assuming  $\alpha \approx 1$  due to the low compressibility of water, and rearranging Eqs. (11), (14), (18), (19), and (23) to eliminate  $M_2$ ,  $r_e$ , and  $P_g$ , one can get a set of equations about  $M_1$  and  $r_0$  as follows:

$$P_1 M_1^2 + \frac{\rho C^2}{2M_1^2} - P_e + 2\gamma \sqrt{\frac{\rho(c_p \Delta T + \Delta H_{l-g}) \ln(R / r_0)}{\epsilon_r \epsilon_0 r_0 \Phi_0^2}} = 0 \quad (24)$$

$$P_e \left[ \frac{\epsilon_r \epsilon_0 \Phi_0^2}{\rho r_0 (c_p \Delta T + \Delta H_{l-g}) \ln(R / r_0)} \right]^{k_s} - P_1 - \frac{\rho C^2}{2M_1^2} - \gamma \sqrt{\frac{\rho(c_p \Delta T + \Delta H_{l-g}) \ln(R / r_0)}{\epsilon_r \epsilon_0 r_0 \Phi_0^2}} = 0 \quad (25)$$

For water vapor,  $\alpha_s$  can be assumed to be 1.3.<sup>27</sup> For high-temperature underwater discharges, the translational plasma temperature was measured to be between approximately 4000 K and 6500 K.<sup>28</sup> An average value of 5000 K was used for  $\Delta T$  in the present study. Figure 6 shows the Mach number of filament propagation,  $M_1$ , as a function of  $\Phi_0$  and  $R$ . The propagation velocity was about 50 km/s, which was higher than the secondary streamer velocity of 25 km/s reported by Baumung and Bluhm<sup>13</sup>, but lower than the value of 200 km/s reported by Woodworth et al.<sup>24</sup> The discrepancy in the two

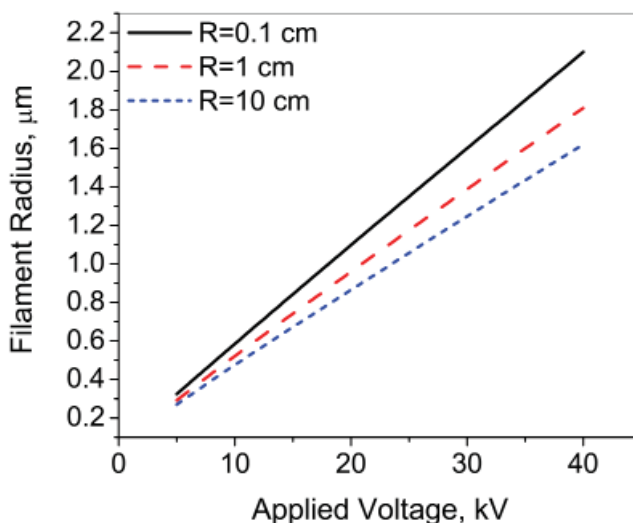


**FIGURE 6.** Variations of filament radius as a function of applied voltage and interelectrode distance.

measurements probably came from the different techniques used for the velocity measurements. The value of  $M_1$  remained constant for various values of  $\Phi_0$  and  $R$ , indicating that the propagation velocity of the streamers was independent of either the applied voltage or interelectrode distance. A similar phenomenon was observed previously,<sup>13,24</sup> where the propagation velocity of secondary streamers was constant over a wide voltage range. Figure 7 shows the filament radius as a function of  $\Phi_0$  and  $R$ . The radius increased slightly as the streamers approached the other electrode, while it decreased almost linearly as the applied voltage dropped. The absolute value of  $r_0$  was about one order smaller than that obtained from the electrostatic model. This could be understood if one considers the energy requirements for the two mechanisms. For the evaporation of water, the energy needed to break the hydrogen bonds between water molecules should be much greater than that required to displace the same volume of water.

The different models based on the electrostatic force and evaporation gave different results of the streamer propagation speed and filament radius. The electrostatic model showed streamers with a larger radius and a lower Mach number, while the thermal model demonstrated that the streamers could move much faster, but were thinner than those determined from the electrostatic model. The different findings from the two models led us to postulate that different mechanisms might be associated with the different modes of the streamer propagation. At the initial primary streamer mode before any significant heat was generated, the electrostatic force might have played a major role. The appearance of the secondary streamer required more time, during which the electron energy could be transferred to the translational energy of water molecules, and subsequently evaporation could become the dominant force to drive the filament to move forward. The transition time between the primary and secondary streamers was on the order of 100 ns,<sup>13</sup> a value that is in accordance with the heating time as estimated above.

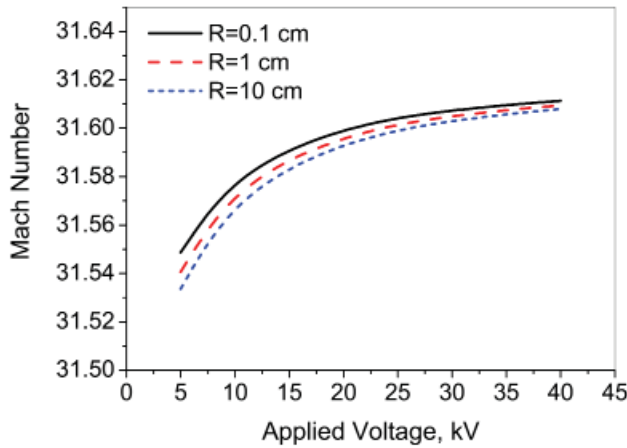


**FIGURE 7.** Variations of the Mach number of a streamer as a function of applied voltage and interelectrode distance.

### III. STABILITY ANALYSIS

The breakdown process is usually characterized by two features, i.e., an initial development of thin discharge channels and a subsequent branching of these channels into complicated “bushlike” patterns. Apparently, the branching process is associated with the instability of the filament. In this section, the linear stability analysis of the axisymmetric perturbation of a filament surface with a certain electric charge density is presented. As long as the wavelength of the perturbation is much smaller than the length of the filament, the stability characteristics can be approximated by considering perturbations to a charged cylinder of constant radius as shown in Figure 8. The peak-to-peak amplitude and wave number of the disturbance are  $h$  and  $k$ , respectively.  $H$  is the depth of wave influence, and  $u$  is the velocity of liquid relative to the disturbance. Then, the surface of the perturbation can be represented by the following equation:

$$r = r_0 + \frac{h}{2} \exp(ikz + \omega t) \quad (26)$$

where  $\omega$  is the oscillation frequency of the instability. To analyze the linear stability, the disturbance of the local electrostatic force, surface tension, and hydrodynamic pressure were considered following a geometrical perturbation. Generally, the surface tension tends to minimize the surface area and subsequently stabilize the disturbance, while the local enhancement of the electrostatic force tended to push the disturbance to grow. In the reference frame that moves together with the tip of the filament, the effects of these three forces were considered separately for the pressure balance between the crest and trough along the streamline (see Fig. 8).

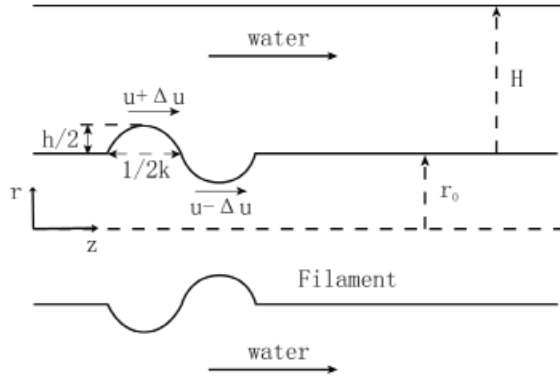


**FIGURE 8.** Schematic diagram of disturbance at the surface of a filament.

### A. Electrostatic Pressure

According to Eqs. (6)–(9), the electrostatic pressure is proportional to the square of the local curvature of the interface, which is different at the crest and trough of the perturbation. Thus, the electrostatic pressures at the crest and trough,  $P_{E,c}$  and  $P_{E,t}$ , become, respectively,

$$P_{E,c} = \epsilon_r \epsilon_0 \Phi_0^2 \frac{\chi_c^2}{4} \quad (27)$$

and

$$P_{E,t} = \epsilon_r \epsilon_0 \Phi_0^2 \frac{\chi_t^2}{4} \quad (28)$$

where  $\epsilon_r$  is the relative permittivity of water, and  $\chi_c$  and  $\chi_t$  are the mean curvatures at the crest and trough, respectively. The expression for the mean curvature can be written as<sup>29</sup>

$$\chi = \frac{1}{r\sqrt{1+(\partial_z r)^2}} - \frac{\partial_z(\partial_z r)}{(1+(\partial_z r)^2)^{3/2}} = \frac{1}{r} - \partial_z(\partial_z r) \quad (29)$$

Substituting Eq. (26) into Eq. (29), one can get expressions for  $M_c$  and  $M_t$ ,

$$\chi_c = \frac{1}{r_0 + h/2} + \frac{h}{2} k^2 \quad (30)$$

$$\chi_t = \frac{1}{r_0 + h/2} - \frac{h}{2} k^2 \quad (31)$$

Subsequently,  $P_{E,c}$  and  $P_{E,t}$  can be written as

$$P_{E,c} = \varepsilon_r \varepsilon_0 \Phi_0^2 \frac{\mathcal{K}_c^2}{4} = \varepsilon_r \varepsilon_0 \Phi_0^2 \left( \frac{1}{(2r_0 + h)^2} + \frac{hk^2}{2(2r_0 + h)} \right) \quad (32)$$

$$P_{E,t} = \varepsilon_r \varepsilon_0 \Phi_0^2 \frac{\mathcal{K}_t^2}{4} = \varepsilon_r \varepsilon_0 \Phi_0^2 \left( \frac{1}{(2r_0 - h)^2} - \frac{hk^2}{2(2r_0 - h)} \right) \quad (33)$$

Thus, the electrostatic pressure difference between the crest and trough becomes

$$\Delta P_E = P_{E,c} - P_{E,t} = -\frac{\varepsilon_r \varepsilon_0 \Phi_0^2 h}{2r_0^3} + \frac{\varepsilon_r \varepsilon_0 \Phi_0^2 hk^2}{2r_0} \quad (34)$$

## B. Surface Tension

The pressures due to the surface tension across the interface at the crest and trough can be written as

$$P_{T,c} = \gamma \mathcal{K}_c = \gamma \left( \frac{1}{r_0 + h/2} + \frac{h}{2} k^2 \right) \quad (35)$$

and

$$P_{T,t} = \gamma \mathcal{K}_t = \gamma \left( \frac{1}{r_0 - h/2} - \frac{h}{2} k^2 \right) \quad (36)$$

Thus, the pressure difference due to surface tension between the crest and trough becomes

$$\Delta P_T = P_{T,c} - P_{T,t} = -\frac{\gamma h}{r_0^2 - h^2/4} + \gamma h k^2 \quad (37)$$

Since  $r_0 \gg h$ , the above equation can be simplified as

$$\Delta P_T = -\frac{\gamma h}{r_0^2} + \gamma h k^2 \quad (38)$$

## C. Hydrodynamic Pressure

When there is a disturbance on the interface of the filament, the flow speed of liquid will be perturbed in the depth of wave influence, inducing a hydrodynamic pressure difference  $\Delta P_H$  between the crest and trough,

$$\Delta P_{HD} = \frac{1}{2} \rho \left( u + \frac{\Delta u}{2} \right)^2 - \frac{1}{2} \rho \left( u - \frac{\Delta u}{2} \right)^2 = \rho u \Delta u \quad (39)$$

where  $\Delta u/2$  is the perturbation in the flow speed caused by the shape of the wave. The dynamic pressure is related to the flow speed through Bernoulli's equation. The pressure difference from the electrostatic force and dynamic effect of the flow has the opposite sign due to the surface tension. For a balance between two kinds of oppositely directed pressure differences, one has

$$\rho u \Delta u + \frac{\gamma h}{r_0^2} - \gamma h k^2 - \frac{\epsilon_r \epsilon_0 \Phi_0^2 h}{2r_0^3} + \frac{\epsilon_r \epsilon_0 \Phi_0^2 h k^2}{2r_0} = 0 \quad (40)$$

In order to solve Eq. (40), the perturbed flow speed  $\Delta u$  must be expressed in terms of experimentally measurable quantities. The following derivation was inspired by Kenyon.<sup>30</sup>

Assuming that the perturbed flow speed is constant over the depth of wave influence, the mass conservation equation through vertical cross sections between the crest and trough becomes

$$\left(u + \frac{\Delta u}{2}\right) \left(H - \frac{h}{2}\right) = \left(u - \frac{\Delta u}{2}\right) \left(H + \frac{h}{2}\right) \quad (41)$$

where  $H$  is the depth of wave influence. The above equation can be reduced to

$$u \cdot h = \Delta u \cdot H \quad (42)$$

The theoretical expression for  $H$  was given by Kenyon<sup>31</sup> as

$$H = \frac{1}{2\pi k} \quad (43)$$

Using Eqs. (42) and (43) to eliminate  $H$  and  $\Delta u$ , Eq. (40) becomes

$$\rho \omega^2 = k \left( \gamma k^2 + \frac{\epsilon_r \epsilon_0 \Phi_0^2}{2r_0^3} - \frac{\gamma}{r_0^2} - \frac{\epsilon_r \epsilon_0 \Phi_0^2 k^2}{2r_0} \right) \quad (44)$$

Since this is a quadratic equation, there will be two different branches of the dispersion relation, and an instability occurs if  $Re(\omega) > 0$ . The first thing to note in Eq. (44) is that when the applied voltage  $\Phi_0$  is equal to zero and the surface is flat, in other words, when the radius of the filament  $r_0$  goes to infinity, the above equation reduces to  $\rho u^2 = \gamma k$ , which is the equation for the classic 2D Rayleigh instability.

Figure 9 shows the instability growth rate  $\omega$  at a low applied voltage, where the process is in Rayleigh mode. The dashed line represents the classic Rayleigh instability for  $\Phi_0 = 0$  and  $r_0 \rightarrow \infty$ . For  $\Phi_0 \neq 0$  and  $r_0$  is finite, instability only happens at high wave numbers. When the voltage increases under this mode, the growth rate is decreased until fully suppressed at a certain critical value. The physical explanation for this can be as follows. The Rayleigh instability occurs due to surface tension, which always acts to break a cylindrical jet into a stream of droplets; on the other hand, the electrostatic force, which is proportional to the square of the applied voltage, always acts in the opposite direction of the surface tension. When the applied voltage increases, the Rayleigh instability would be suppressed when the two forces are balanced.



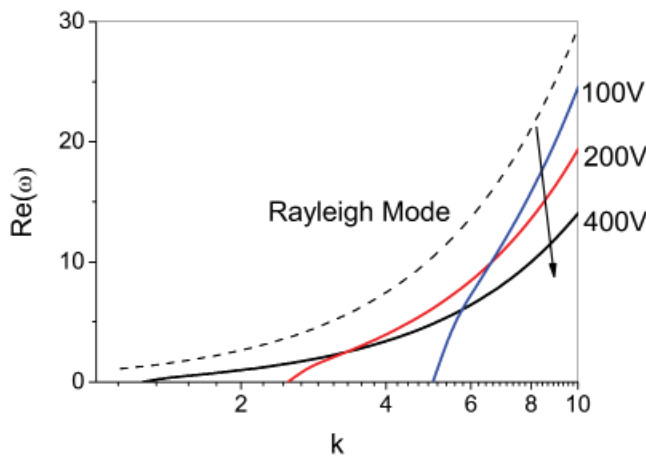


**FIGURE 9.** Instability growth rate  $\omega$  at low applied voltages;  $k$  and  $\omega$  are nondimensionalized using streamer radius  $r_0$  and time scale  $t = (\rho r_0^3/\gamma)^{1/2}$ .

As the voltage continues to increase, the instability enters the electrostatic mode, where the electrostatic force exceeds the force created by the surface tension and becomes the dominant force. Figure 10 shows the instability growth rate  $\omega$  at a high voltage. Both the growth rate and the range of wave number increase as the voltage rises. The physics of this mode is a consequence of the interaction of the electric field with the surface charge on the interface; surface tension is a parameter of less importance for this mode. The mechanism for the instability is that a perturbation in the radius of the filament induces a perturbation in the surface charge density and therefore a perturbation in the electrostatic pressure. At a high voltage, the perturbation is amplified by the fact that the electrostatic pressure  $P_E$  is proportional to  $\Phi^2$ , causing the instability. In contrast to the Rayleigh mode, the instability in the electrostatic mode is unavoidable at low wave numbers (long wavelength). This may explain why the filament always tends to branch into bushlike structures.

#### IV. CONCLUSIONS

The electric breakdown of water involves both the generation and propagation of low-density channels through the liquid. The different physical processes and interactions between different phases of the media should contribute to the complexity of the problem. In the present study, different modes of the streamer propagation were considered in simplified steps, with each step characterized by a driving force and the corresponding hydrodynamic drag. The effects of the electrostatic force and local heating on the streamer propagation were analyzed using simplified assumptions. It was shown that both of them were dominant for the streamer propagation, but at different time scales. Furthermore, a linear instability analysis was performed on a charged cylindrical streamer in an external electric field to understand the bushlike growth pattern of breakdown in

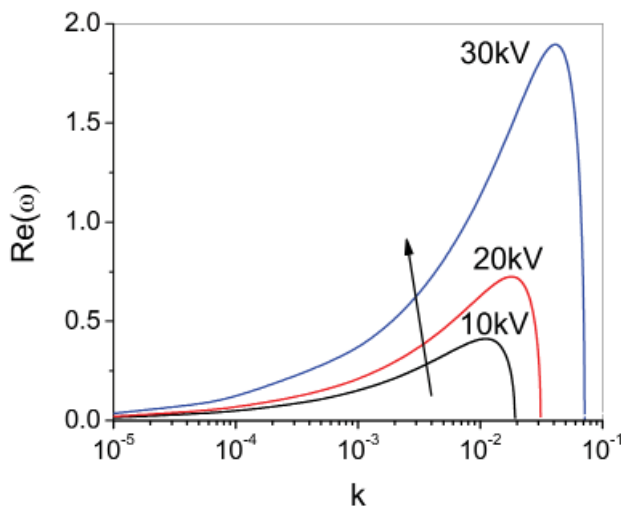


**FIGURE 10.** Instability growth rate  $\omega$  at high applied voltages;  $k$  and  $\omega$  are nondimensionalized as in Figure 9.

the liquid. It was shown that the stability may be caused by the competition between perturbations in the electrostatic pressure and surface tension caused by the disturbance of the streamer geometry. With increasing applied voltage, the electrostatic instability was found to grow, whereas the classic Rayleigh instability was found to be suppressed.

## ACKNOWLEDGMENT

This work was supported by U.S. Department of Energy, National Energy Technology Laboratory, through Contract No. DE-NT0005308.

## REFERENCES

1. Locke B, Sato M, Sunka P, Hoffman MR, Chang J-S. Electrohydraulic discharge and non-thermal plasma for water treatment. *Ind Eng Chem Res.* 2006;45:882–905.
2. Sunka, P. Pulse electrical discharges in water and their applications, *Phys Plasmas.* 2001;8:2587–94.
3. Akiyama H. Streamer discharges in liquids and their applications. *IEEE Trans Dielectr Electr Insul.* 2000;7:646–53.
4. Zahn M, Ohki Y, Fenneman DB, Gripshover RJ, Gehman VH. Dielectric properties of water and water/ethylene glycol mixtures for use in pulsed power system design. *Proc IEEE.* 1986;74:1182–221.
5. Aprile E, Ku WH-M, Park I. Delta electron production and the ultimate energy resolution of liquid argon ionization detectors. *IEEE Trans Nucl Sci.* 1988;35:37–41.
6. Laroussi M. Nonthermal decontamination of biological media by atmospheric-pressure plasmas: review, analysis, and prospects. *IEEE Trans Plasma Sci.* 2002;30:1409–15.

7. Beroual A. Electronic and gaseous processes in the prebreakdown phenomena of dielectric liquids. *J Appl Phys.* 1993;73:4528–33.
8. Jones HM, Kunhardt ES. Development of pulsed dielectric breakdown in liquids. *J Phys D.* 1995;28:178–88.
9. Lewis T. A new model for the primary process of electrical breakdown in liquids. *IEEE Trans Dielectr Electr Insul.* 1998;5:306–15.
10. Lewis T. Breakdown initiating mechanisms at electrode interfaces in liquids. *IEEE Trans Dielectr Electr Insul.* 2003;10:948–55.
11. Qian J, Joshi RP, Kolb J, Schoenbach KH, Dickens J, Neuber A, Krompholz H, Schamiloglu E, Gaudet J. Microbubble-based model analysis of liquid breakdown initiation by a sub-microsecond pulse. *J Appl Phys.* 2005;97:113304.
12. Qian J, Joshi RP, Schoenbach KH, Woodworth JR, Sarkisov G. Model analysis of self- and laser-triggered electrical breakdown of liquid water for pulsed-power applications. *IEEE Trans Plasma Sci.* 2006;34:1680–91.
13. An W, Baumung K, Bluhm H. Underwater streamer propagation analyzed from detailed measurements of pressure release. *J Appl Phys.* 2007;101:053302.
14. Watson P, Chadbank W. The role of electrostatic and hydrodynamic forces in the negative-point breakdown of liquid dielectrics. *IEEE Trans Electr Insul.* 1991;26:543–59.
15. Lisitsyn IV, Nomiya H, Katsuki S, Akiyama H. Thermal processes in a streamer discharge in water. *IEEE Trans Dielec Dielectr Electr Insul.* 1999;6:351–6.
16. Joshi RP, Qian J, Zhao G, Kolb J, Schoenbach KH, Gaudet J, Schamiloglu E. Are microbubbles necessary for the breakdown of liquid water subjected to a submicrosecond pulse? *J Appl Phys.* . 2004;96:5129–39
17. Kupershtokh AL, Medvedev DA. Anisotropic instability of dielectric liquids and decay to vapor-liquid system in strong electric fields. *Tech Phys Lett.* 32:634–7, 2006
18. Fridman A, Kennedy L. *Plasma physics and engineering.* New York: Taylor & Francis Group; 2006.
19. Morch KA. Reflections on cavitation nuclei in water. *Phys Fluids.* 2007;19:072104.
20. Gidalevich E, Boxman R. Sub- and supersonic expansion of an arc channel in liquid. *J Phys D.* 2006;39:652–9.
21. Sunka P, Babicky V, Clupek M. Generation of chemically active species by electrical discharges in water. *Plasma Sources Sci Technol.* 1999;8:258–265.
22. Lama W, Gallo C. Systematic study of the electrical characteristics of the trichel current pulses from negative needle-to-plane coronas. *J Appl Phys.* 1977;45:103–13.
23. Beroual A, Zahn M, Badent A, Kist K, Scwabe AJ, Yamashita H, Yamazawa K, Danikas M, Chadband WD, Torshin Y. Propagation and Structure of Streamers in liquid Dielectrics. *IEEE Electr. Insul. Mag.,* 14:6–14, 1998
24. Woodworth JR, Lehr J, Elizondo-Decanini J, Miller PA, Aragon B, Elizondo-Decanini J, Fowler W, Maenchen JE, Sarkisov GS, Corley J, Hodge K, Drennan S, Guthrie D, Mowrer D, Navarro M, Johnson DL. Optical and Pressure Diagnostics of 4-MV Water Switches in the Z-20 Test Facility. *IEEE Trans. Plasma Sci.,* 32:1778–89, 2004
25. White FM. *Viscous fluid flow*, 3rd ed.. Singapore: McGraw-Hill; 2006.
26. Itikawa Y. Electron-impact vibrational excitation of H<sub>2</sub>O. *J Phys Soc Jpn.* 1974;36:1127–32.

27. Parry W, Bellows J, Gallagher J, Harvey A. ASME international steam tables for industrial use. New York: ASME; 2008.
28. Lange H, Huczko A. Carbon arc discharge: plasma emission spectroscopy and carbon nano-structure formation. *Trans Mater Res Soc Jpn.* 2004;29:3359–64.
29. Eggers J. Nonlinear dynamics and breakup of free-surface flows. *Rev Mod Phys.* 1997;69: 865–930.
30. Kenyon KE. Capillary waves understood by an elementary method. *J Oceanogr.* 1998;54: 343–6.
31. Kenyon KE. On the depth of wave influence. *J Phys Oceanogr.* 1983;13:1968–70.